THE JOURNAL OF PHYSICAL CHEMISTRY B

Article

pubs.acs.org/JPCB

Morphological and Rheological Insights on Polyimide Chain Entanglements for Electrospinning Produced Fibers

Stefan Chisca, Andreea Irina Barzic,* Ion Sava, Niculae Olaru, and Maria Bruma

"Petru Poni" Institute of Macromolecular Chemistry, Aleea Grigore Ghica Voda 41A, Iasi-700487, Romania

ABSTRACT: Solution rheology and electrospinning performance of an aromatic polyimide based on 3,3′,4,4′-benzophenonetetracarboxylic dianhydride (BTDA) and 3,3′-dimethyl-4,4′-diaminodiphenylmethane (MMDA) was studied. Analyzing the dependence of specific viscosity on polymer concentration enabled the evaluation of the transition from semidilute unentangled to semidilute entangled regime at 18.3%. Modification of chain interactions in solution is also reflected in a sudden increase of flow energetic barrier and consistency index values from 3.56 to 10.28 kJ/mol and 0.19 to 1.09 Pa·s^n, respectively. In the concentration domain of 15−20% the relaxation time is enhanced from 0.48 to 1.07 s, as a consequence of less chain mobility, which can be associated with the elastic character of the polyimide solution, useful for obtaining fibers. Scanning electron microscopy (SEM) and polarized light microscopy (PLM) images indicate that at 25% beaded fibers are obtained, while at 30% bead-free fibers are formed having the diameter comprised between 0.56 and 0.85 μm.

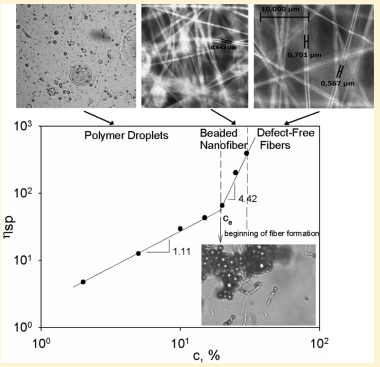

INTRODUCTION

Membrane-based gas separation processes have been recognized as effective and economical approaches in some applications of gas treatments. Among high-performance polymers used in this area, aromatic polyimides (PIs) have received a great deal of attention because of their excellent separation characteristics and high thermal and chemical stability, as well as mechanical strength.[1−3] Transport processes in PI membranes depend on their selectivity and permeability, which can be controlled through the physical and chemical properties. Generally, PI chain rigidity determines the selectivity, while interchain spacing and chain mobility governs the permeability of membranes. In the molecular design of PIs, the main factors affecting the gas transport properties are (1) spatial linkage configurations, (2) type of bridging groups, and (3) bulkiness and polarity of pendant groups of the polymer chain. In this context, many reports were focused on designing new PI membranes by using bulky monomers,[4−6] grafting and halogenation of polyimide backbone,[7−9] cross-linking treatments,[10,11] thermal annealing,[12] blending with compounds exhibiting complementary properties,[13,14] and introduction of nano-organic fillers.[15,16]

The technology of membrane fabrication also advanced significantly with the development of new materials during the past two decades. In fact, without a breakthrough in fabrication, the applications of newly invented high-performance membrane materials would be very limited. Several major advances in membrane fabrication took place, such as gradient dense-layer membranes,[17] defect-free ultrahigh flux asymmetric membranes,[18] and ultrathin high-performance hollow fiber membranes.[19,20]

There are two routes which can be used for the fabrication of PI fibers: (1) the spinning of a PI precursor solution, followed by chemical or thermal imidization of filaments,[21] and (2) the dry or wet spinning of PI solutions. The fibers produced by traditional techniques (e.g., melt, wet, and dry spinning) typically range from 5 to 100 μm[22,23] in diameter. Smaller values can be achieved by using a recent technique, which involves application of an electric field between a capillary tip and a collector, produced by a high-voltage source, namely, electrospinning.[24] The main advantage of this method is the ability to produce fast ultrafine fibers from polymer liquids (solution or melt) in a simple and relatively inexpensive fashion. Because of the extremely small diameters and excellent uniformity of electrostatically spun fibers, these materials have porosities and large surface-to-area ratios[25] that make them more suitable candidates as filters and membranes,[26] wound dressings and vascular grafts,[27] composite reinforcements,[28] and nanoelectronics.[29]

The electrospinning process can be manipulated by a number of variables. The parameters that control the process are solution properties (flow rate), electric field strength, needle tip design, and ambient parameters such as temperature and humidity.[30−32] A predominant role is played by solution properties such as viscosity, conductivity, surface tension, polymer molecular weight, dipole moment, and dielectric constant. It has been shown for many polyimide/solvent systems that increasing the solution concentration or viscosity reduces the number of bead defects and increases the overall fiber diameter of the electrospun fibers.[33−35] Moreover, researchers have electrospun polyimide solutions with varying concentration resulting in viscosities that ranged over 1 order of magnitude and reported the resulting fiber structure.[36−39] However, more detailed investigations of the dependence of

Received: March 28, 2012
Revised: June 20, 2012
Published: July 5, 2012

fiber morphology on solution rheological behavior in the literature are not reported. For instance, the influence of the chain overlap concentration (c^*) or the entanglement concentration (c_e) for a given system on the electrospinning process is not reported. The establishment of these parameters is very important because the jet breaks up into droplets if the concentration (and hence the viscosity) of the solution is not suitable (i.e., no entanglement of the polymer chains takes place).

Some PIs have an inherently rigid chain structure, which reduces the amount of chain entanglements in solution.[40,41] Among the aromatic tetracarboxylic dianhydrides used as raw materials for PIs, 3,3′,4,4′-benzophenonetetracarboxylic dianhydride (BTDA) has a semiflexible character which might reduce the viscosity and thus could enhance the electrospinnability of the solution. In this work, the fiber-forming ability of an aromatic PI based on BTDA and 3,3′-dimethyl-4,4′-diaminodiphenylmethane (MMDA) is investigated. The aim of the paper is to study the correlation between solution properties and solid phase characteristics, providing insight on the interactions from the system, which lead to the formation of the resulting fiber morphology. As a consequence, a good knowledge on the rheological properties of these solutions is important for their handling and formulation, and also for finding the optimal conditions of processing the polyimide into thin fibers by electrospinning.

EXPERIMENTAL SECTION

Materials. *N*,*N*′-Dimethylacetamide (DMAc) (Merck) and anhydrous lithium chloride (Fluka) were used as received. Benzophenonetetracarboxylic dianhydride from Aldrich was purified by recrystallization from acetic anhydride (mp 225−226 °C), and 3,3′-dimethyl-4,4′-diaminodiphenylmethane was obtained in our laboratory by a previously reported method (mp 155−157 °C).[42,43]

Preparation of Polyimide and Solutions. The method of two step polycondensation reaction has been used for the synthesis of the investigated polyimide. The first step of the polycondensation reaction was performed at room temperature with equimolar amounts of benzophenonetetracarboxylic dianhydride and 4,4′-diamino-3,3′-dimethyldiphenylmethane in DMAc, at a total concentration of 11%. The mixture was continuously stirred under nitrogen for 6 h to obtain the polyamidic acid (PAA). The second step consists in thermal imidization of the resulting polyamidic solution in the same reaction flask by heating at reflux temperature for 4 h, under a slow stream of nitrogen to remove the water of imidization. The final product was precipitated in water, washed with water and ethanol, and then dried in a vacuum oven at 105 °C. The structure of the investigated polyimide is shown in Scheme 1.

A standard procedure for preparing the sample solutions was used. First, the polymer powder was weighed and put into a jar (also weighed). Then, the polymer was mixed at room temperature with an appropriate amount of *N*,*N*-dimethylacetamide (DMAc), to obtain 2%, 5%, 10%, 15%, 20%, 25%, and 30% concentrations. These solutions were used in rheological measurements and for obtaining electrospun fibers.

Scheme 1. Structure of the Polyimide

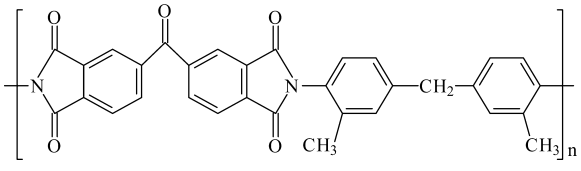

Measurements. FTIR spectra were recorded with a FT-IR VERTEX 70 (Bruker Optics Company), with a resolution of 0.5 cm^{-1}.

The rheological properties of the concentrated mixed solutions were determined on a Bohlin CS50 instrument, manufactured by Malvern Instruments. The measuring system presents cone−plate geometry with a cone angle of 4° and a diameter of 40 mm. Shear viscosities were registered over the 0.07−3000 s^{-1} shear rate domain for surprising all possible flow regimes, at several temperatures (25−55 °C). During the oscillatory shear tests, the frequency was varied between 0.01 and 15 Hz, and a shear stress of 2 Pa was applied.

For obtaining of the electrospun fibers we used an electrospinner, equipped with a KD Scientific syringe pump and a high voltage source. The electrospinning apparatus was composed of several components: a high-voltage supplier (Gamma High Voltage Research, E3 30P-5W), a capillary tube with a stainless steel needle, a syringe pump (Harvard Apparatus), and a stainless steel collecting screen. A high electric field from the high-voltage supplier is generated between the needle and the collection plate. As it reaches a certain voltage difference, the electrical charge passing through the polymer solution overcomes surface tension of the polymer solution droplet that is formed at the tip of the needle. Electrospinning was carried out using a syringe with a 1.2 mm diameter spinneret at an applied voltage difference of 15−20 kV over the distance of 15 cm, and the syringe pump was set to deliver the solution at a flow rate of 1.5 mL/h.

Polarized light microscopy (PLM) images were obtained with a Leica DM 2500 M microscope. The morphology of the polyimide fibers was investigated by scanning electron microscopy (SEM) using a Quanta 200 ESEM.

RESULTS AND DISCUSSION

Here we investigated a polyimide based on benzophenonetetracarboxylic dianhydride and 4,4′-diamino-3,3′-dimethyldiphenylmethane with respect to its ability to be processed into fibers by electrospinning technique. This polyimide showed the weight-average molecular weight of 52000 g/mol and polydispersity of 2.08.

The imide structure of the polyimide fibers was identified by FTIR spectra. Figure 1 presents the FTIR spectra for fibers obtained at 25% concentration untreated and thermally treated at 250 °C. Both spectra exhibit the presence of characteristic absorption bands for carbonyl group of the imide ring at about 1780 and 1716−1720 cm^{-1}, and characteristic band for C−N vibration at 1370 and 720 cm^{-1}, which prove the formation of imide rings.[44] An additional band at 3423 cm^{-1} was observed in the spectrum of untreated 25% concentration sample and was attributed to amide groups of residual solvent *N*,*N*′-dimethylacetamide. The intensity of this absorption band completely disappears in the spectrum of the corresponding treated sample due to elimination during the thermal treatment of residual solvent that had remained in the process of obtaining fibers. Also, in these spectra are shown the characteristic absorption bands for the methyl groups at about 2920 cm^{-1}, for the methylene groups at about 2850 cm^{-1} and at around 1670 cm^{-1} for C═O stretch from the benzophenone unit.

dx.doi.org/10.1021/jp302957r | J. Phys. Chem. B 2012, 116, 9082−9088

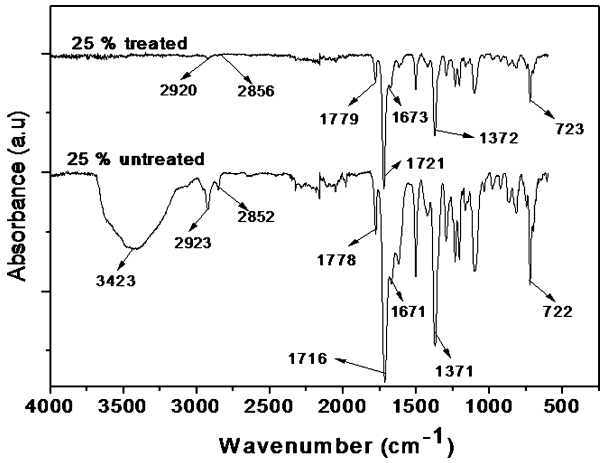

Figure 1. FTIR spectra for polyimide fiber obtained from a solution of 25% concentration.

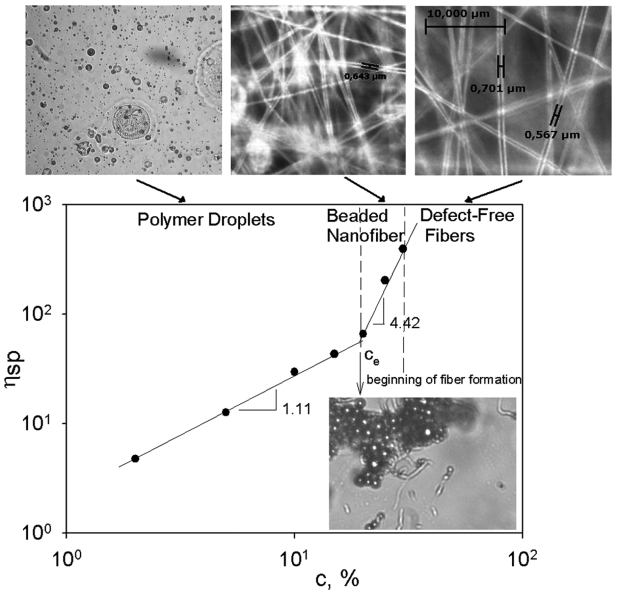

Figure 2. Dependence of specific viscosity on concentration and corresponding developed morphology of polyimide examined by PLM at 5%, 20%, 25%, and 30%.

The properties of the polymer solution have a major influence on the electrospinning process. The present paper discusses the importance of certain major solution properties, such as viscosity of the solution, the amount of chain entanglements, and the conformation of the polymer chains in solution, in correlation with the developed morphology.

Chain Entaglements' Effect on Flow and Viscoelastic Behavior. Viscosity, which measures the resistance of the fluid to flow, plays an important role in electrospinning, since it stabilizes the jet. Viscosity is a function of the concentration of solution and of the molecular weight of the polymer. This relationship has an accelerating pitch, which can follow a power law equation.[45] The concentration, the molecular weight, and the viscosity form a trinity of parameters, all affecting the fiber forming ability of the solution, and also termed electrospinnability. According to McKee[46] and Shenoy[47] the chain entanglements can be used instead of these three parameters when evaluating fiber formation, since a certain amount of chain entanglement is needed to keep the solution jet coherent during the electrospinning.

The rheological behavior of the polyimide was investigated on a wide concentration range in order to identify the different concentration regimes in which polymer chain entanglements dominate the flow behavior. The dilute concentration regime, where the polymer chains are distributed randomly as separate spheres, was not studied since in this domain no interchain entanglements occur. In this case, separated chains behave more or less independently, and the polymer molecules primarily interact with the solvent molecules.[48] Therefore, the working polymer solution concentrations used in the rheological measurements were in the range of 2−30%. In the semidilute range, Colby and co-workers[49−51] showed that there are two different power law dependences. For neutral linear polymers in a good solvent, specific viscosity $\eta_{sp} \sim c^{1.25}$ in semidilute unentangled regime and $\eta_{sp} \sim c^{4.25-4.5}$ in semidilute entangled domain.[52] The η_{sp} as a function of concentration is plotted in Figure 2 for polyimide in DMAc. At low concentrations $\eta_{sp} \sim c^{1.11}$ indicating the onset of the semidilute unentangled, where the concentration is large to have some chain overlap, but not enough to cause any significant degree of entanglement. As a result, the developed morphology of the sample, observed by polarized light microscopy (PLM), is similar to polymer droplets. As the concentration is further increased, the topological constraints induced by the larger occupied fraction of the available hydrodynamic volume in solution introduce chain entanglements. The change in the slope $\eta_{sp} \sim c^{4.42}$ marks the semidilute entangled regime. The crossover of concentration from the semidilute unentangled to semidilute entangled regime, referred to as the critical entanglement concentration, c_e, was found to be 18.30%. Below c_e the solution viscosity is controlled by the intramolecular excluded-volume effects, while above c_e the intermolecular entanglements have a dominant effect on the rheology of the solution[49] enabling the formation of beaded fibers, observed in the concentration range of 18.3−25%. The literature[46] shows that the almost double value of c_e is the optimum concentration for the formation of bead-free fibers. In the case of the studied polyimide at the concentration of 30%, which is approximately 2 times c_e, the amount of chain entanglements increases sufficiently to produce bead-free fibers. This result is confirmed by PLM and SEM images recorded for different concentrations, which show that only at 30% the bead defects are no longer observed.

The shear rate sweeps from 0.07 to 3000 s^{-1} were performed on studied PI solutions at various concentrations. All samples showed shear thinning behavior, followed by a Newtonian plateau at shear rates higher than 10 s^{-1}. According to Figure 3, at low concentrations (2−15%) the polyimide solutions present a high slope of the shear thinning domain. The randomly distributed chains are separated, thus leading to low internal friction and to high orientation of the chains under the effect of the shear field. When the concentration increases, the chains exhibit smaller mobility in solution as a consequence of more entanglement formation, thus preventing the chain ordering and the reduction of viscosity. This observation is reflected in the decrease of the slope corresponding to the thinning range, starting with the concentration of 20%, at which the entanglements slightly begin to dominate the flow behavior. At the highest concentration of 30% the transition from thinning region to Newtonian domain is very small, indicating that the amount of entanglements is high enough to produce

dx.doi.org/10.1021/jp302957r | J. Phys. Chem. B 2012, 116, 9082−9088

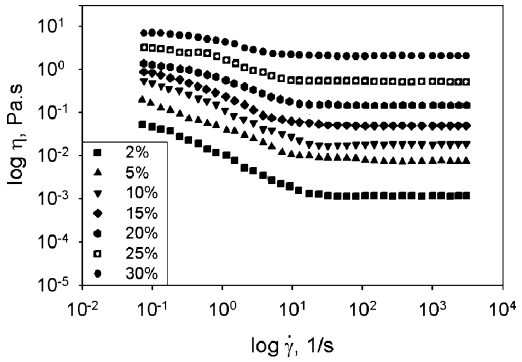

Figure 3. Logarithmic plot of viscosity as a function of shear rate for polyimide at different concentrations.

polyimide fibers, as supported by optical microscopy data (Figure 2).

The existence of polymer entanglement interactions, which strongly determine the electrospinnability, can also be described by the flow activation energy, E_a. This parameter is derived from the dependence of viscosity on temperature, which can be described by Arrhenius relationship (eq 1),

$$\eta_0 = A \cdot \exp(E_a/RT) \quad (1)$$

where η_0 is the zero shear viscosity ($\eta_0 = \lim \dot{\gamma}_{\to 0}(\eta)$), A is the pre-exponential factor, T is the absolute temperature, and R is the universal gas constant.

Linearization of eq 1 allows determination of the flow activation energy from the slope of the straight line of ln η_0 versus $1000/T$ (Figure 4), which is equal to $E/1000\ R$. For the

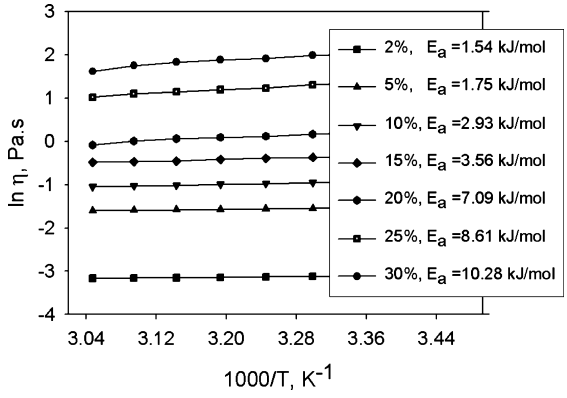

Figure 4. Logarithmic plot of viscosity (ln η) versus reciprocal temperature for polyimide solutions at 0.1 s^{-1} and different concentrations. Flow activation energy as a function of concentration.

calculation of E_a the viscosity was selected at a shear rate close to zero (0.1 s^{-1}), where the first 2−3 points from Figure 3 are almost independent of shear rate. However, if the term ln η_0 is taken from Newtonian regime and then extrapolated to zero shear rate, the values of E_a are similar.

A smaller value of E_a implies a lower energy barrier for the movement of polyimide segments in the solvent. In the case of polymer solutions under analysis here, this barrier can be related to the interaction between the chains and can be determined by polymer entanglements. Figure 4 shows the plot of ln η versus reciprocal temperature for investigated polyimide solutions. It can be observed that PI solutions follow the Arrhenius expression from eq 1 and the flow activation energy is influenced by concentration regimes. The obtained values of E_a are in correlation with the changes recorded on viscosity. In other words, in the range of 2−15% the activation energy is comprised between 1.54 and 3.56 kJ/mol, revealing that the few interactions among polymer chains do not affect their mobility, consequently the threshold of flow is lower. In this concentration domain the lack of entanglements leads to a beaded structure instead of fibers. At concentrations higher than 20%, the formation of entanglements generates a higher energetic flow barrier, therefore flow activation energy values start to increase rapidly from 3.56 kJ/mol for 15% polymer concentration to 10.28 kJ/mol for 30% polymer concentration. This sudden increase in flow energy barrier indicates that the concentration of 30% is optimal for stabilizing the jet during the electrospinning process.

For polyimide solutions the dependence of shear stress, σ, on shear rate, $\dot{\gamma}$, in the pseudoplastic domain, obeys the power law relationship described by eq 2,

$$\sigma = K \cdot \dot{\gamma}^n \quad (2)$$

where n and K are the flow behavior and consistency indices, respectively.

In the studied concentration domain, the shape of curves representing log shear stress versus log shear rate plots is different, as observed in Figure 5, where two flow regimes are

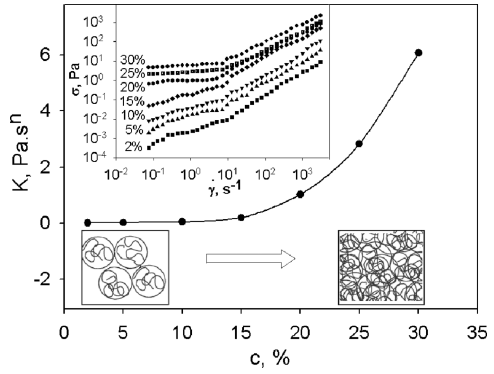

Figure 5. Variation of consistency index (K) with concentration (c) for polyimide solutions at room temperature. The small graphic represents the double-logarithmic plot of shear stress (σ) versus shear rate ($\dot{\gamma}$).

distinguished. Therefore, the flow curves exhibit two regions characterized by different slopes. In the first part of Figure 5, over the shear rate range of 0.07−10 s^{-1}, the power law index, n, is lower than unity as expected for a non-Newtonian shear-thinning (pseudoplastic) behavior. In this region the values of n are decreasing from 0.631 to 0.109, when the concentration increases from 2% to 30%. After the shear rate of 10 s^{-1}, the shear stress of all samples becomes linear, having the slope of 1.02−1.10 highlighting the Newtonian behavior. The resulting values of consistency indices of the polyimide solutions in DMAc are determined from the linear regression corresponding to non-Newtonian flow. Figure 5 shows that the flow consistency index increases with concentration. The fluidity of the investigated samples exhibits a pronounced variation at the limit between the semidilute unentangled to semidilute entangled regime, revealing a consistency suitable for preparation of fibers by electrospinning.

Physical chain entanglements behave in a similar manner as chemical cross-links, although chains can slide past one another affecting the viscoelastic behavior, as well. This can be evaluated

dx.doi.org/10.1021/jp302957r | J. Phys. Chem. B 2012, 116, 9082−9088

from oscillatory rheometry measurements, which allow characterization of the frequency dependence of the polyimide solutions. In this controlled-strain test, the samples are deformed in oscillatory shearing flow up to reach a maximum strain, which is small enough to be in the linear regime. For polyimide in 1−4 Pa domain the storage (G') and loss (G'') moduli are independent of the shear stress. Therefore, a shear stress of 2 Pa was selected in order to perform the oscillatory shear measurements in the linear viscoelastic region. The variation of the viscoelastic moduli as a function of the oscillatory frequency (ω) at 25 °C for investigated solutions is shown in Figure 6.

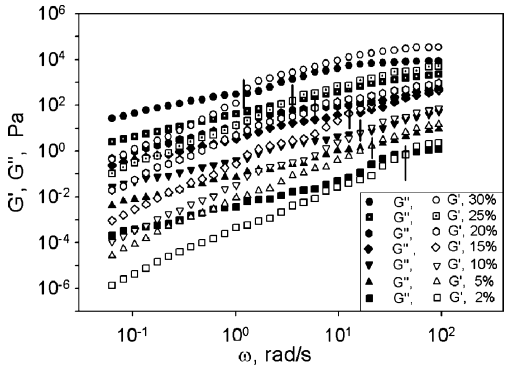

Figure 6. Double logarithmic plot of shear moduli (G' and G'') versus angular frequency (ω) at different concentrations. For a better visualization of the crossover frequency the graphs were shifted.

The viscoelastic behavior can be described by the Maxwell model, expressed through eq 3,

$$\sigma + \lambda \frac{\partial \sigma}{\partial t} = \eta \dot{\gamma} \tag{3}$$

where λ (the relaxation time) and η are the model parameters.

As can be observed from the above equation and from Figure 6, the sample response at very low frequencies G'' scales with $\omega^{1.02-1.2}$ and G' scales with $\omega^{1.91-2.04}$, without any plateau appearing in G' versus ω curves (except the solution of 30%). In this frequency range the loss modulus is always higher than the elastic one signifying viscous response. At high frequencies the storage modulus (elastic) becomes greater than the loss (viscous) modulus. In other words, at low angular frequencies the liquid-like behavior prevails as a result of unrecoverable viscous loss, while at high angular frequencies the solid-like character becomes predominant and determines energy reversibility stored in the sample as a result of the number and strength of interactions from the system. At the highest studied concentration (30%) the dominant elastic response is seen in a small rubbery region, where the storage modulus shows a plateau. Literature data[53] indicate that the plateau region appears for polymers with entanglements in solution.

As it is well-known, three zones terminal, plateau, and transitions delimited by two points for which $G' = G''$ can be distinguished for a viscoelastic liquid in the double logarithmic plot of shear moduli as a function of frequency.[54] This behavior results from the interaction number and the effect of entanglements of polymer chains. Two sets of relaxation times can be distinguished: the long-range relaxation, λ_1, which occurs at the time scale of the terminal zone and the short-range relaxation at the time scale of the transition zone, λ_2. The crossover frequency (ω_c) values for which $G' = G''$ are inversely proportional with the relaxation times. For the studied solutions, only the longest relaxation time was determined by using the crossover frequency from Figure 6. Modification of the chain interactions in solution are reflected in the values of crossover point, which delimits the viscous flow from the elastic flow. The overlap frequency increases with decreasing concentration. This can be explained more easily in terms of relaxation time, which is a measure of the rate at which the global structure changes in response to the change in flow. Thus, with changing flow, the degree of anisotropy changes with the speed and time duration of the flow. When returning to the quiescent state (no flow), the liquid relaxes to the original global isotropic condition. The force of reorientation to the isotropic condition of rigid microstructural elements is due to Brownian motion, while shape recovery of flexible microstructural elements is aided by internal springs. The larger the local structures, the longer the relaxation time. Therefore, at small concentrations (2−15%) where the random coils are separated by solvent molecules, the chain mobility is high and the time required for reducing the stress in solution by flow is low. In the concentration domain of 15−20%, where the transition from semidilute unentangled to semidilute entangled regime occurs, the relaxation time suddenly increases from 0.48 to 1.07 s (Table 1). The large values of λ_1 imply a limitation of the chain motions at large scale, which can be associated with the elastic character of the polyimide solution, useful for obtaining fibers.

Table 1. Relaxation Time (λ) and tan δ Values for Polyimide Solutions

c, %	λ_1, s	tan δ at ω_c
2	0.14	0.15
5	0.30	0.65
10	0.39	0.88
15	0.48	0.93
20	1.07	1.86
25	2.27	1.95
30	4.85	2.03

The relative amount of energy loss in the material during cyclic stress in oscillatory testing is evaluated from tan δ values (Table 1). The favorable interactions among the chains decrease the free volume in solution, so that the polymer behavior becomes more elastic, and the intensity of tan δ decreases. Therefore, the formation of chain entanglements prevents the dissipation of energy and preserves mechanical properties in solution optimum for fiber preparation.

Morphology of Polyimide Fibers. Generally, during the electroprocessing of polymer solutions, it has been established that an increase in polymer concentration results in the following progression of the fiber morphology: (1) beads only, (2) beads with incipient fibers, (3) beaded fibers, (4) fibers only, and (5) globular fibers/macrobeads. For the investigated polyimide, the developed morphology at different concentrations was investigated by SEM. The results derived from the micrographs shown in Figure 7 are consistent with data obtained by rheological measurements, revealing that the amount of chain entanglements is one of the main factors that influence the fiber morphology.

In Figure 7a it is observed that the lack of chain entanglements leads to the formation of a beaded structure with the diameter size in the range of 2−5 μm at 15%

dx.doi.org/10.1021/jp302957r | J. Phys. Chem. B 2012, 116, 9082−9088

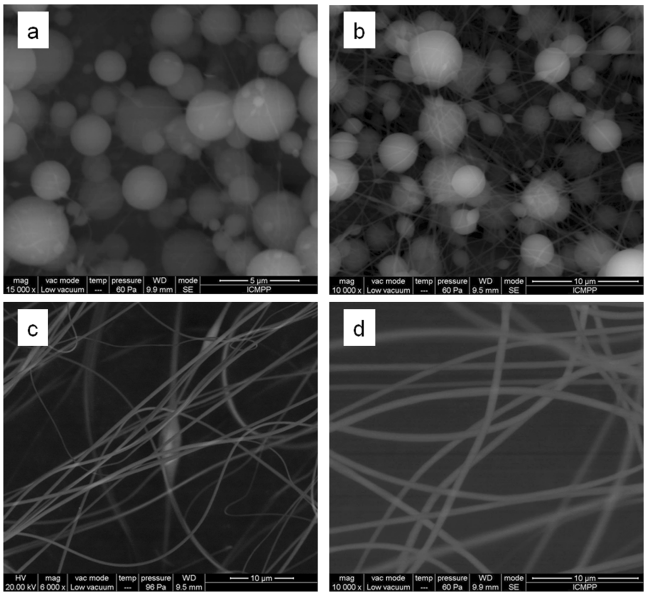

Figure 7. SEM images of the polyimide morphology at different solution concentrations: (a) 15%; (b) 20%; (c) 25%; (d) 30%.

concentration and also of few pseudofibers. Figure 7b presents the morphology at 20% concentration, which is a little higher than the critical entanglement concentration of 18.30%, as calculated from rheological measurements. At this concentration a mixture of beads with incipient fibers and beaded fibers was obtained. Up to this concentration the chain mobility in solution decreases due to more chain entanglements, and this aspect influences the morphology of the polyimides processed by electrospinning. As can be seen from Figure 7c, at 25% concentration the fibers are formed probably because the entanglements are high enough. Even at this concentration some bead defects can be observed, but fewer than in the case of 20% concentration. The fiber diameter is in the range from 0.30 to 0.58 μm. At the highest concentration of 30%, polyimide fibers without defects with the diameter in the range of 0.60−0.85 μm are obtained. The small diameter of the bead-free polyimide fibers makes these materials suitable for membrane separation applications.

CONCLUSIONS

Chain entanglements are one of many parameters that can significantly influence fiber formation during polymer electrospinning. In order to understand how many entanglements are required to affect/stabilize fiber formation, a semiempirical analysis of transition from electrospraying to electrospinning in the good solvent was elaborated. The implications of the semidilute unentangled and semidilute entangled concentration regimes on the electrospinning process were determined for a solution of polyimide, based on benzophenonetetracarboxylic dianhydride and 4,4′-diamino-3,3′-dimethyldiphenylmethane in *N*,*N*′-dimethylacetamide as solvent. The changes in the slope of specific viscosity dependence on concentration from 1.11 to 4.42 at critical entanglement concentration c_e = 18.3% reflect the appearance of entanglements. These modifications also enhance the flow energetic barrier and the solution consistency, inducing a stability of the jet during electrospinning. Oscillatory test shows that all studied samples present a viscoelastic behavior. At 30% the elastic behavior becomes more dominant, as revealed by the presence of a small rubbery region due to formation of chain entanglements. Morphological investigations were done in correlation with rheological measurements. The results show that critical entanglement concentration c_e of 18.3% was the minimum concentration required for electrospinning of beaded nanofibers, while approximately double value of c_e, i.e., 30%, was the minimum concentration required for electrospinning of uniform, bead-free fibers.

AUTHOR INFORMATION

Corresponding Author

*"Petru Poni" Institute of Macromolecular Chemistry, Aleea Grigore Ghica Voda 41A, Iasi-700487, Romania. Tel: (40) 232 217 454. Fax: (40) 232 211 299. E-mail: irina_cosutchi@yahoo.com.

Notes

The authors declare no competing financial interest.

ACKNOWLEDGMENTS

This work was financially supported by PN II-RU project, code TE_221/2010, no. 31/10.08.2010.

REFERENCES

(1) Hsiao, S. H.; Chen, Y. J. *Eur. Polym. J.* **2002**, *38*, 815−828.
(2) Matsumoto, T. *J. Photopolym. Sci. Technol.* **2001**, *14*, 725−730.
(3) Mathews, A. S.; Kim, I.; Ha, C. S. *Macromol. Symp.* **2007**, *344*, 249−250.
(4) Wang, R.; Cao, Y.; Vora, R.; Tucker, R. J. *J. Appl. Polym. Sci.* **2001**, *82*, 2166−2173.
(5) Bruma, M.; Hamciuc, E.; Yampolskii, Yu. P.; Alentiev, A. Yu.; Ronova, I. A.; Rozhkov, E. M. *Mol. Cryst. Liq. Cryst.* **2004**, *418*, 11−19.
(6) Vidyakin, M. N.; Lazareva, Yu. N.; Yampolskii, Yu. P.; Alentiev, A. Yu.; Ronova, I. A.; Bruma, M.; Hamciuc, E.; Lungu, R. *Polym. Sci., Ser. A* **2007**, *49*, 1045−1052.
(7) Kharitonov, A. P.; Mokvin, Y. L.; Syrtsova, D. A.; Starov, V. M.; Teplyakov, V. V. *J. Appl. Polym. Sci.* **2004**, *92*, 6−17.
(8) Carey, F. A. *Organic chemistry*; McGraw Hill: New York, 2006.
(9) Guiver, M. D.; Robertson, G. P.; Dai, Y.; Bilodeau, F.; Kang, Y. S.; Lee, K. J.; et al. *J. Polym. Sci., Part A* **2003**, *40*, 4193−4204.
(10) Askari, M.; Xiao, Y.; Li, P.; Chung, T.-S. *J. Membr. Sci.* **2012**, *390−391*, 141−151.
(11) Kita, H.; Inada, T.; Tanaka, K.; Okamoto, K. *J. Membr. Sci.* **1994**, *87*, 139−147.
(12) Kawakami, H.; Mikawa, M.; Nagaoka, S. *J. Membr. Sci.* **1996**, *118*, 223−230.
(13) Coleman, M. R.; Kohn, R.; Koros, W. J. *J. Appl. Polym. Sci.* **1993**, *50*, 1059−1064.
(14) Kapantaidakis, G. C.; Kaldis, S. P.; Dabou, X. S.; Sakellaropoulos, G. P. *J. Membr. Sci.* **1996**, *110*, 239−247.
(15) Li, F.; Li, Y.; Chung, T. S.; Kawi, S. *J. Membr. Sci.* **2010**, *356*, 14−21.
(16) Zhang, Q.; Wu, D.; Qi, S.; Wu, Z.; Yang, X.; Jin, R. *Mater. Lett.* **2007**, *61*, 4027−4030.
(17) Kesting, R. E.; Fritzsche, A. K.; Cruse, A.; Murphy, M. K.; Handermann, A. C.; Malon, R. F.; Moore, M. D. *J. Appl. Polym. Sci.* **1990**, *40*, 1557−1574.
(18) Koros, W. J.; Clausi, D. T. *J. Membr. Sci.* **2000**, *167*, 79−89.
(19) Chung, T. S.; Teoh, S. K.; Hu, X. *J. Membr. Sci.* **1997**, *133*, 161−175.
(20) Shieh, J. J.; Chung, T. S. *J. Membr. Sci.* **2000**, *166*, 259−269.
(21) Goponenko, A. V.; Hou, H.; Dzenis, Y. A. *Polymer* **2011**, *52*, 3776−3782.
(22) Xiang, H. B.; Huang, Z.; Liu, L. Q.; Chen, L.; Zhu, J.; Hu, Z. M.; Yu, J. R. *Macromol. Res.* **2011**, *19*, 645−653.
(23) Fay, C. C.; Hinkley, J. A.; St. Clair, T. L.; Working, D. C. *Adv. Perform. Mater.* **1998**, *5*, 193−200.

(24) Yang, K. S.; Edie, D. D.; Limc, D. Y.; Kimd, Y. M.; Choia, Y. O. *Carbon* **2003**, *41*, 2039−2046.
(25) Shin, Y. M.; Hohman, M. M.; Brenner, M. P.; Rutledge, G. C. *Polymer* **2001**, *42*, 9955−9967.
(26) Gibson, P. W.; Shreuder-Gibson, H.; Rivin, D. *Colloids Surf., A* **2001**, *187*−*188*, 469−481.
(27) Buchko, C. J.; Chen, L. C.; Shen, Y.; Martin, D. C. *Polymer* **1999**, *40*, 7397−407.
(28) Burgshoef, M. M.; Vancso, G. J. *Adv. Mater.* **1999**, *11*, 1362−1365.
(29) Norris, I. D.; Shaker, M. M.; Ko, F. K.; MacDiarmid, A. G. *Synth. Met.* **2000**, *114*, 109−114.
(30) Fong, H.; Reneker, D. H. *Structure formation in polymeric fibers*; Hanser: Munich, Germany, 2001.
(31) Huang, Z. M.; Zhang, Y. Z.; Kotaki, M.; Ramakrishna, S. *Compos. Sci. Technol.* **2003**, *63*, 2223−2253.
(32) Reneker, D. H.; Yarin, A. L. *Polymer* **2008**, *49*, 2387−2425.
(33) Ren, J.; Li, Z.; Wong, F. S.; Li, D. *J. Membr. Sci.* **2005**, *248*, 177−188.
(34) Askari, M.; Xiao, Y.; Li, P.; Chung, T. S. *J. Membr. Sci.* **2012**, *390*−*391*, 141−151.
(35) Li, F.; Li, Y.; Chung, T. S.; Kawi, S. . *J. Membr. Sci.* **2010**, *356*, 14−21.
(36) Nah, C.; Han, S. H.; Lee, M. H.; Kim, J. S.; Lee, D. S. *Polym. Int.* **2003**, *52*, 429−432.
(37) Zhao, X.; Wang, C.; Cheng, Y.; Chen, W.; Zhu, M. *Colloid Polym. Sci.* **2010**, *288*, 1471−1477.
(38) Chen, S.; Han, D.; Hon, H. *Polym. Adv. Technol.* **2011**, *22*, 295−303.
(39) Chen, F.; Bera, D.; Banerjee, S.; Agarwal, S. *Polym. Adv. Technol.* **2012**, *23* (6), 951−957.
(40) Cosutchi, A. I.; Hulubei, C.; Ioan, S. *J. Macromol. Sci. B* **2007**, *46*, 1003−1012.
(41) Cosutchi, A. I.; Hulubei, C.; Ioan, S. *J. Polym. Res.* **2010**, *17*, 541−550.
(42) Lu, Q. H.; Yin, J.; Xu, H. J.; Zhang, J. M.; Sun, L. M.; Zhu, Z. K.; Wang, Z. G. *J. Appl. Polym. Sci.* **1999**, *72*, 1299−1304.
(43) Sava, I. *Mater. Plast.* **2006**, *43*, 15−19.
(44) Sava, I.; Chisca, S.; Bruma, M.; Lisa, G. *J. Therm. Anal. Calorim.* **2011**, *104*, 1135−1143.
(45) Kenawy, E. R.; Bowlin, G. L.; Mansfield, K.; Layman, J.; Simpson, D. G.; Sanders, E. H.; Wnek, G. E. *J. Controlled Release* **2002**, *81*, 57−64.
(46) McKee, M. G.; Wilkes, G. L.; Colby, R. H.; Long, T. E. *Macromolecules* **2004**, *37*, 1760−1767.
(47) Shenoy, S. L.; Bates, W. D.; Frisch, H. L.; Wnek, G. E. *Polymer* **2005**, *46*, 3372−3384.
(48) Teraoka, I. *Polymer Solutions: An introduction to physical properties*; John Wiley & Sons Inc: New York, 2002.
(49) Krause, W. E.; Bellomo, E. G.; Colby, R. H. *Biomacromolecules* **2001**, *2*, 65−9.
(50) Dobrynin, A. V.; Colby, R. H.; Rubinstein, M. *Macromolecules* **1995**, *28*, 1859−1871.
(51) Bordi, F.; Colby, R. H.; Cametti, C.; Lorenzo De, L.; Gili, T. *J. Phys. Chem. B* **2002**, *106*, 6887−6893.
(52) de Gennes, P. G. *Scaling Concepts in Polymer Physics*; Cornell University Pres: Ithaca, NY, 1979.
(53) Lomellini, P. *Polymer* **1992**, *33*, 1255−1260.
(54) Hsieh, T. T.; Tiu, C.; Simon, G. P.; Wu, R. Y. *J. Non-Newtonian Fluid Mech.* **1999**, *86*, 15−35.